Assessment of the impact of tidal power extraction from the Eastern Scheldt storm surge barrier through the evaluation of a pilot plant

Anton de Fockert [a,*], Arnout C. Bijlsma [a], Tom S.D. O'Mahoney [a], Wilbert Verbruggen [a], Peter C. Scheijgrond [b], Zheng B. Wang [c]

[a] *Hydraulic Engineering, Deltares, 2629 HV, Delft, the Netherlands*
[b] *Bluespring, 3012 GH, Rotterdam, the Netherlands*
[c] *Marine and Coastal Systems, Deltares, 2629 HV, Faculty of Civil Engineering and Geosciences, Delft University of Technology, Delft, the Netherlands*

ARTICLE INFO

ABSTRACT

Hydraulic structures can be a promising place for tidal energy extraction due to the high flow velocities, easy access to the power grid and easy access for maintenance. However, quantification of the impacts of a tidal power plant in a hydraulic structure is not straight forward. In 2015 a pilot plant consisting of an array of five Tocardo tidal turbines was installed in the Eastern Scheldt Storm Surge Barrier in the Netherlands. This pilot was accompanied by monitoring studies to verify that the operation of the plant had no adverse impact on the barrier and its surroundings. This paper presents the assessment of the hydraulic impact of the tidal power plant in the storm surge barrier based on an analysis of water level and current measurements, combined with numerical modeling and followed by an assessment of the environmental impact with emphasis on the effects on the intertidal areas in the estuary. This validation approach by a pilot plant is imperative to understand the interaction between tidal turbines and the hydraulic structure on the local scale. This understanding gives extra credibility to the predictions of the extrapolated large-scale and large array assessments which will always be fully numerical.

1. Introduction

In order to reduce the carbon dioxide emissions, many countries work hard to increase the sustainable energy share of their energy mix. Besides hydropower, wind and solar power are two of the most applied sources of renewable energy. However, as these fluctuating energy sources induce challenges to the power grid, there is an urgent need for more predictable energy resources. Marine energy resources such as wave energy, tidal energy, thermal energy conversion and salinity gradients could contribute to the energy mix, from which the latter three are more predictable energy sources. The worldwide tidal energy potential is estimated at about 500–1000 TWh/y [1], of which only a small part can be exploited due to economical constraints. One of the most promising countries for the use of tidal energy is the United Kingdom. Pelc and Fujita [2] estimated that the potential for the UK may reach up to 50 TWh/y, which is half of the total potential of Western Europe and half the need of the UK [3]. Due to the moderate tidal current velocities in the North Sea near the Dutch coast, tidal energy exploitation focuses

on existing hydraulic structures. Near or in discharge sluices and storm surge barriers velocities are higher, making it economically viable to harvest tidal energy [4].

Tidal energy converters (TEC) may impact the environment in different ways [5]. Potential impacts that have been identified include collision risks and acoustic disturbance for fish and sea mammals, and further disturbance of sediment dynamics. However, quantification in real projects is rarely undertaken due to the small scale of existing tidal energy projects. In 2010 Shields et al. [6] discussed the poor understanding of the ecological implications of altering hydrodynamics due to marine energy devices. To further scale-up and commercialize tidal power, the impacts should be quantified, which requires detailed environmental impact studies per project. Existing studies to date are considering the environmental impact of large TEC arrays in open sea sites, exclusively by means of numerical modelling. These studies do not consider the turbines and the turbine structures in detail, as these local effects are considered negligible compared to the large-scale impacts. For this reason, they implemented the tidal farm in their numerical

models as energy sinks. Due to the large potential for tidal energy extraction in the UK, multiple researchers investigated the impact of tidal energy extraction around the UK focusing on the areas with large potential. The Pentland Firth has one of the largest potentials in the UK, with lease agreements up to 398 MW for the MeyGen site. Therefore, Chatzirodou et al. [7] assessed the impact on the sedimentary budget of a 400 MW tidal energy farm near the island of Stroma. They found that the impact of the tidal farm exceeds the morphological change under natural hydrodynamic conditions. It was concluded that the morphological change scales with the amount of energy extraction. This was also found by Fairley et al. [8] when studying the cumulative morphodynamic effects of four large tidal arrays with a rated power of about 100–200 MW per farm. Robins et al. [9] investigated the impact of tidal energy extraction on the sediment transport near the Skerries (northwest of Anglesey) in the Irish sea. They modelled different sizes of TEC arrays and found that arrays with a capacity up to 50 MW had a small impact on the sediment patterns compared to the natural variability. Their model showed that tidal arrays with a capacity greater than 50 MW could significantly impact the sediment processes up to e.g. 10 km from the TEC array. In 2012, Neill et al. [5] assessed the tidal farm with a capacity of 300 MW in the Alderney Race near Normandy by means of a numerical model. This study showed that a full-scale TEC array would have an impact on the sediment budget near the headland. The studies above consider mainly the morphological impact due to the turbines, while other studies assess the change in impact by varying spacing and placement of the turbines ([10–12]). Ahmadian et al. [10] investigated the placement of large TEC arrays of 1000 turbines with a rated power of 150 MW in different layouts in the Bristol channel. They found that the layout of the turbine array can have a significant impact on the power output and to a lesser extent on the hydrodynamics. Fallon et al. [11] did a similar assessment of large-scale arrays in the highly dynamic Shannon Estuary. They studied the impact of 600 turbines (rated power 180 MW) and found that the impact reduced with lower turbine densities (i.e. increased spacing between turbines). The impacts were considered not significant with a spacing of 5 rotor diameters or more between turbines. Plew et al. [12] showed that the power production of tidal energy sites with 100 turbines may reduce significantly due to site constraints. For the Tory Channel in New Zealand it was concluded that the maximum likely power would be 1/3 of the power predicted by analytical models, due to limited depth and economic constraints such as placing turbines in locations with optimal site conditions. Besides these studies where spacing of the turbines had been investigated, Ramos et al. [13] and Sanchez [14] studied the impact of tidal turbines in highly dynamic estuaries in the Galician Rias in the north of Spain near the Galician coast. Ramos et al. [13] considered a small tidal energy farm in Ria de Ribadeo consisting of 8 turbines. They found that the resistance of the tidal farm increased flow velocities around the farm and reduced the velocities through the farm. This caused a 10–20% power reduction of the turbines. Sanchez et al. [14] showed that the impact of a tidal farm in the flood dominant dynamic tidal estuary Ria de Ortigueira might be larger during ebb than during flood, which requires the need for detailed understanding of the estuarine circulation. González-Gorbeña et al. [15] investigated the optimal size of a tidal array in a multi-inlet system in the south of Portugal considering hydrodynamic and morphological constraints. They formulated four multi objective optimization models subject to a set of performance and environmental constraints of the whole system. With this approach they identified the optimal array rows and the number of TEC converters per row and used this in a validated hydrodynamic model to determine the impact of the TEC arrays.

It should be noted that the installed capacity in most numerical models discussed above (in the order of hundreds of MW and hundreds of turbines) is very significant for tidal power, considering the global installed capacity of tidal stream power is less than 12 MW in 2020 [16]. The schematization of turbines as energy sinks for modelling in the above studies is of questionable validity when the turbines are located close to or in a hydraulic structure. The interaction between the TEC array and the hydraulic structure could impose additional impacts on the performance of the hydraulic structure which normally has other functions than extracting energy. This is also the case for the positioning of the turbines in a hydraulic structure, as the exact positioning of the turbines might influence the flow patterns in and around the hydraulic structure.

This article describes the method and results to understand the impact of tidal energy extraction from a hydraulic structure by studying a tidal power pilot plant in the Eastern Scheldt Storm surge barrier in the Netherlands. Detailed flow and water level measurements were carried out prior to the installation of the plant and during operation. By means of these measurements in combination with detailed CFD simulations, the impact on the hydraulic structure and its bed protection was quantified. Furthermore, these results were used for the parametrization of the tidal turbines in the large-scale numerical model to assess the impact of upscaling tidal power from the hydraulic structure.

Flow velocities up to 5 m/s in the gates of the barrier make this location well suited for tidal power extraction. Another advantage of the application of free stream tidal turbines in a barrier is the easy access and close connection to the power grid. The Eastern Scheldt is an ecologically vulnerable estuary with tidal channels and tidal flats. Added resistance on the flow through the barrier due to tidal power extraction may impact the morphology and ecology in the estuary. For a relatively small-scale pilot, the impact may be too small to measure. However, upscaling the tidal power extraction to multiple gates of the barrier requires careful investigation.

Part of the permit for this pilot plant which is installed and operated by Tocardo, was a mandatory monitoring of the biotic and abiotic ecosystem as well as parameters that affect the stability of the storm surge barrier itself. From permit perspective and societal impact, various assessments were required by stakeholders and the consenting body Rijkswaterstaat to assess the impact of the pilot plant [17]. These studies consisted of 1) monitoring of water levels, to assess the impact of the pilot plant on the tidal range in the estuary, 2) assessing the flow velocities near the turbines based on ADCP measurement data and assessing the impact of the turbines on the discharge through the gate, 3) assessing the impact on the bed protection, 4) monitoring the effect on the pillar construction by annual deformation measurements and analysis on failure probability and 5) assessing the impact on sea mammals by analyzing swim patterns and blunt trauma of stranded mammals.

This article discusses the first three items discussed above, as these items are mostly related to each other. The turbine manufacturer and Rijkswaterstaat agreed on changes in failure probability after deformation measurements of the pillar construction. These structural impacts are not further described. The impact of the turbines on the sea mammals was assessed by Wageningen Marine Research (WMR) for a period of 2 years [17]. The behavior of the harbor seals, grey seals and harbor porpoises was monitored during the operation of the pilot plant in Gate 8. In addition, pathological examination has been carried out on stranded mammals. The assessment showed no trend effect on the behavior of these mammals and from the pathological examination it was not possible to determine if observed blunt trauma was caused by the tidal turbines or by collision with other protrusions such as fishing equipment.

The assessments described above considered both nearfield and far-field impacts. The near field assessments focused on the reduced flow through the barrier and the impact of the changed flow patterns near the bed protection. The large-scale assessments focus on the main intertidal flats in the estuary. This article presents a brief description of the estuary and the pilot plant, after which the impacts are addressed based on the measurements from the monitoring campaign and the numerical models which were validated against these measurements [18]. At the end of this article the potential for upscaling tidal power from the storm surge barrier is discussed based on the conclusions of the impact of this pilot plant compared to other impacts such as sea level rise.

2. Eastern Scheldt estuary

2.1. Tidal system

The Eastern Scheldt estuary developed over thousands of years. For centuries, humans tried to reclaim land from the estuary, which was not always successful [20]. The estuary was in dynamic morphological equilibrium prior to the construction of the barrier ([20]).

In 1953 severe flooding in the south of the Netherlands, particularly in the Eastern Scheldt region led to the development of the Delta Plan to protect the low-lying areas of the Netherlands against the sea. The Eastern Scheldt storm surge barrier was one of the last hydraulic structures built under this plan. The Eastern Scheldt barrier contains 62 gates, which allow the tide to enter the estuary. The gates are open during normal weather conditions and closed during severe storm surges.

The Eastern Scheldt barrier consists of 3 sections with different lengths (Fig. 1). The most northern section, called 'Hammen' consists of 15 gates, the center section 'Schaar' consists of 16 gates and the most southern section 'Roompot' (including tidal power station in Gate 8) consists of 31 gates. The storm surge barrier has a varying sill level between −4.5 m NAP (vertical reference datum in the Netherlands, approximately mean sea level at the barrier) and −10.5 m NAP and a top beam at +1 m NAP [24]. The width of each gate is 39.5 m and the width of the pillars is 5.5 m. The bed protection at the barrier consists of armour rock up to 10 tons near the barrier extended with an asphalt mastic section covered with armour rock up to 3 tons. From 200 m onwards block mattresses are present with quarry run rock until the end of the bed protection at approximately 600 m from the barrier [24].

After the construction of the storm surge barrier in 1986 and the construction of the Oesterdam and Philipsdam at the eastern end of the estuary (Fig. 1), the characteristics of the Eastern Scheldt tidal basin changed. Due to the reduced area of the tidal basin and the resistance induced by the barrier, the amount of water flowing in and out of the tidal basin (tidal prism) decreased by 30% and the difference between mean high water and mean low water in the basin (tidal range) reduced by 12% ([25,26]). The installation of the barrier induced large hydraulic and morphological changes in the estuary, which are still ongoing.

Eelkema [20] investigated the morphological behavior of the basin and discussed local erosion and accretion problems caused by the construction of the barrier. The Eastern Scheldt estuary is a multichannel system with meandering ebb and flood channels [21,22]. In between these channels, tidal flats (shoals) are present which are drying at low water, such as the Roggeplaat (RP), the Galgeplaat (GP) and the Neeltje Jans (NJ) in Fig. 1. Because of the reduced tidal volume flowing through the Eastern Scheldt, the old tidal channels were in fact too deep after the construction of the barrier. Over the years, these channels are accreting to reach a new dynamic equilibrium. As the sill and bed protection prevent the sand flux through the barrier, the accretion of the channels takes place at the expense of the adjacent tidal flats. De Vet [23] studied the impact of the barrier on the tidal flats by comparing the Eastern and Western Scheldt estuary and found an opposing development of the flats and large differences in shape of the tidal flats between the two estuaries. The flats in the Western Scheldt have milder slopes compared to the tidal flats in the Eastern Scheldt. The intertidal flats are an important feeding ground for migratory birds and serve as shelter for resting seals. To preserve the tidal flats from eroding further, a large-scale suppletion took place in 2019 on one of the main tidal flats in the Eastern Scheldt, the Roggeplaat [27].

In 2013 a consortium of researchers from Deltares and Wageningen Marine Research (at the time called IMARES) assessed the influence of sea level rise and the effect of the construction of the storm surge barrier on the intertidal area in the Eastern Scheldt. The report, called "the autonomous downward trend" [28] of the Eastern Scheldt, presented an effect chain of stressors and ecosystem services for the estuary. As mentioned before by Shields et al. [6], this insight in the functioning of the marine ecosystem is vital to determine the impact of a marine energy system. Because the tidal turbines in the barrier could be seen as an additional stressor for the ecosystem, the diagram in Fig. 2 has been updated incorporating tidal energy extraction from the barrier. The diagram illustrates that the acreage and quality of the intertidal area are a key aspect for the ecology in the Eastern Scheldt (i.e. birds, shell fish, etc.).
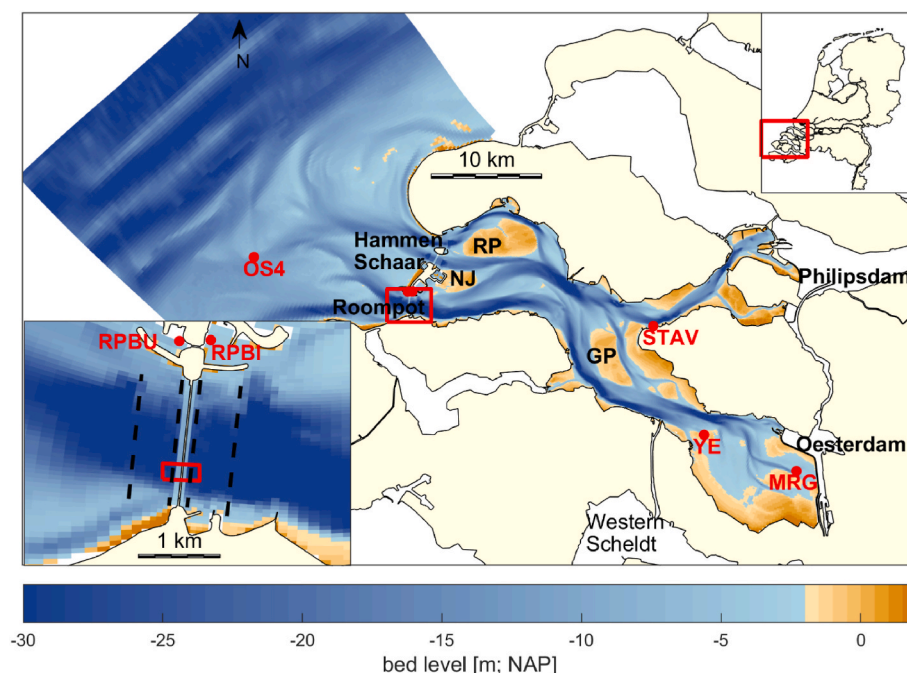

Fig. 1. Location map of the Eastern Scheldt estuary with tidal channels and tidal flats. The bed level of the hydrodynamic model is presented including permanent water level monitoring stations in red (RPBU: Roompot Buiten, RPBI: Roompot Binnen, STAV: Stavenisse, YE: Yerseke, MRG: Marollegat) and the main intertidal flats in black (RP: Roggeplaat, NJ: Neeltje Jans, GP: Galgenplaat). In the lower left figure, the Roompot section of the barrier is shown. The red rectangle in this figure shows the extent of the CFD model. The dashed lines represent 100 m distance from the barrier and the end of the bed protection at 600 m from the barrier.
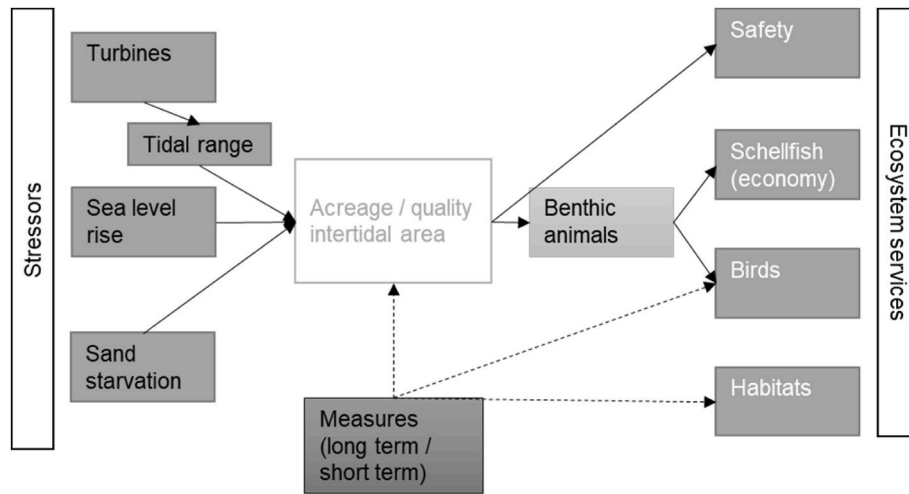
Fig. 2. Effect chain for the Eastern Scheldt with stressors and ecosystem services (obtained from Ref. [28] and adapted for tidal energy extraction from the barrier). The tidal turbines are incorporated in this diagram as stressor. The quality of the intertidal area refers to the time for birds to forage.

2.2. Tidal power plant

Due to the high flow velocities, the gates of the Eastern Scheldt barrier are well suited locations for tidal energy extraction. Rijkswaterstaat, the responsible agency of the Ministry of Infrastructure and Water management, issued permits for two pilot projects with tidal power in two gates of the Roompot Section of the barrier. At the end of 2015, Tocardo installed the tidal power plant in Gate 8 of the barrier (counted from the south) consisting of five tidal turbines (Fig. 3). The width of Gate 8 is 39.5 m, resulting in a maximum opening area of 415 m^2 at high water level. The tidal turbines are mounted on a frame which can rotate to lift all turbines simultaneously out of the water. The Tocardo T200 turbines with a capacity of 250 kW each are equipped

with so called bi-blades (diameter 5.26 m and blockage area of 109 m^2). The passive pitching system allows the turbines to generate energy during both ebb and flood. The tip-speed ratio of the turbines is kept at an optimal operational point by managing the rotational speed of the turbines to generate a maximum amount of energy under varying flow conditions. The annual energy production of the pilot plant between July 2016 and June 2018 (including operational limitations and maintenance) ranged between 700 and 900 MWh.

Rijkswaterstaat must guarantee the proper functioning of the barrier under all circumstances in order to protect the southeastern Delta of the Netherlands against flooding. Any obstruction in the barrier that could compromise the operation needs to be investigated by assessing the change in probability of failure of the barrier. As the tidal turbines
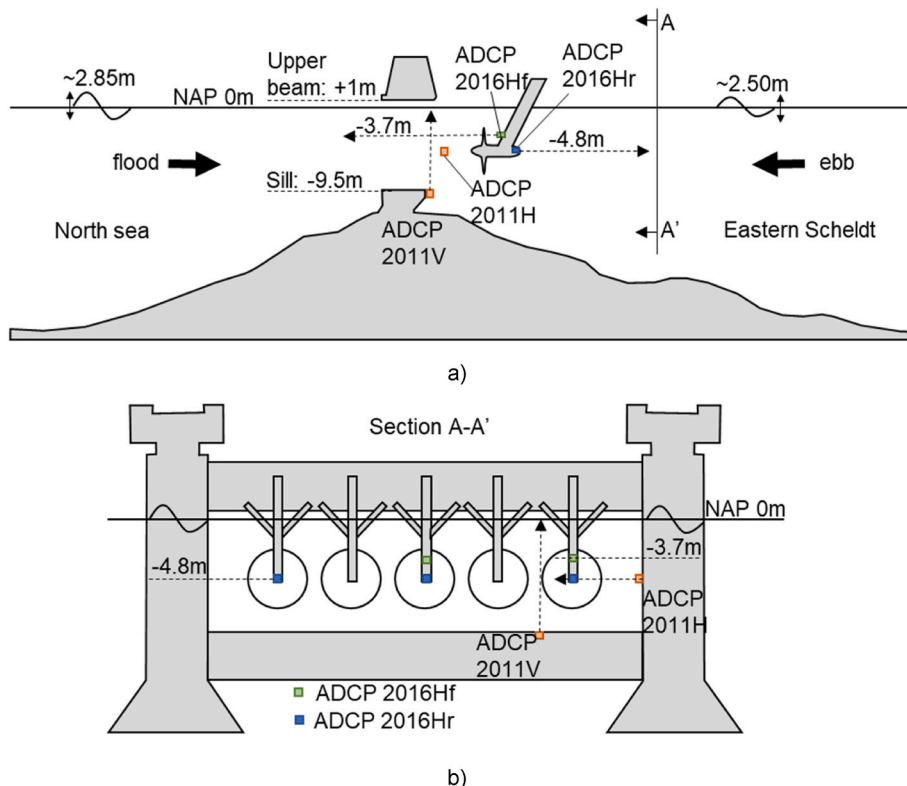

Fig. 3. a A cross section through the middle turbine in Gate 8 of the Roompot Section of the Eastern Scheldt barrier. The location and orientation of the ADCP's on the turbines and the ADCP's applied in 2011 on the barrier are indicated (2011H: horizontal out of plane and 2011V: vertical) and the ADCP's on the turbines in 2016 are indicated by ADCP2016Hf: front ADCP and ADCP2016Hr: rear ADCP. The length of the arrows show the measurement range of the ADCP's. All levels refer to NAP. Fig. 3b: Cross section over the width of Roompot Gate 8.

mounted in the barrier influence the flow patterns downstream of the barrier, the effects of these turbines should be quantified by means of monitoring. To allow the pilot project to extract tidal energy from the barrier, but to avoid compromising on the main function of the barrier, a strict monitoring plan was agreed in which the impact of the tidal turbines could be assessed. The permit for the pilot plant limits the operational window for maximum hydraulic head limits between the measurement stations Roompot Binnen and Roompot Buiten (see Fig. 1). The pilot plant is allowed to operate up to a maximum head (water level difference between Roompot Buiten and Roompot Binnen) of 0.60 m during ebb 0.80 m during flood. These restrictions limit the potential energy extraction for this site where head differences up to 1.1 m occur.

3. Monitoring and modelling

To assess the environmental impact of the tidal power plant in Gate 8 of the Eastern Scheldt barrier, measurements were carried out by both Rijkswaterstaat and Tocardo. These measurements were used to assess the impact of the turbines on the tidal range and to validate of the numerical models.

3.1. Monitoring

3.1.1. Water level measurements

Rijkswaterstaat performs water level measurements at various tidal stations in the Eastern Scheldt on a regular basis and with a 10-min interval. Since the completion of the Storm Surge Barrier in 1986, two of these stations are located near the Roompot section: Roompot Binnen and Roompot Buiten. (Fig. 1). These stations are used for the operation of the barrier and the operation of the tidal turbine array in Gate 8. To investigate the effect of the tidal turbine array on the basin, an analysis was made of the trend of the annual average tidal range with and without tidal power plant. The result can be seen in Fig. 4. Partly due to the operational head limitations as described earlier, the tidal power plant was producing energy for about 50% of the time during the period June 2016–May 2017. The figure shows the effect of the tidal power plant on the tidal amplification factor (ratio of the annual averaged tidal range of Roompot Binnen and Roompot Buiten), which is 0.866 for the indicated period, which is within the range of amplification factors

found in the measured period. Based on these findings, it was concluded that a much longer period of operation is required to determine whether or not there is a statistically significant effect on the annual average tidal range.

3.1.2. Current measurements

To investigate the impact of the tidal turbines on the flow through the gate, velocity measurements were performed prior to and after installation of the tidal turbines (Table 1). In 2011, prior to the installation of the tidal turbines, Partrac, on behalf of Tocardo, carried out ADCP measurements in Gate 8 of the Roompot section of the barrier. One ADCP was mounted at the sill and measured in the direction of the water surface (ADCP 2011V in Fig. 3). This ADCP covered the total water depth at the sill. The other ADCP (ADCP 2011H) was mounted at a height of −4.8m NAP on the pillar between Gates 8 and 9 The signals of ADCP 2011V and ADCP 2011H did not overlap, because the vertical mounted ADCP was located at 9.2 m from the sidewall, while the range of the horizontal ADCP was limited to 8.2 m. The horizontal ADCP's on the tidal turbines were mounted on the strut (ADCP 2016Hf) and in the rear (ADCP 2016Hr) of outer turbines and the middle turbine to measure the flow velocities in streamwise direction, while the ADCP measurements of 2011 measured the flow in lateral direction. The measurement sections of both the horizontal and vertical velocity measurements prior to and after the installation of the tidal power station did not overlap, because the measurements of ADCP 2011H and 2016Hf are at different heights (see Fig. 3a) and because the measurements of ADCP 2011V and 2016Hf are not at the same location (see Fig. 3b), which makes a direct interpretation on the impact of the tidal turbines on the flow patterns and flow through the gate difficult.

For the ADCP measurement on the middle turbine looking towards the barrier (ADCP 2016Hf), a relation was established between the hydraulic head over the barrier based on the water level measurements of the Roompot Binnen and Roompot Buiten and the current velocity at the sill in the gate (see Fig. 5). The same relation is defined for the situation without turbines based on the vertical ADCP data from 2011 (ADCP 2011V) at −3.7 m NAP (see Fig. 3a). Due to inertia, the flow velocity in the gate at increasing head is smaller than during decreasing head. For this reason, both situations were analyzed. Higher velocities were measured at the sill during flood than during ebb. This is mainly caused
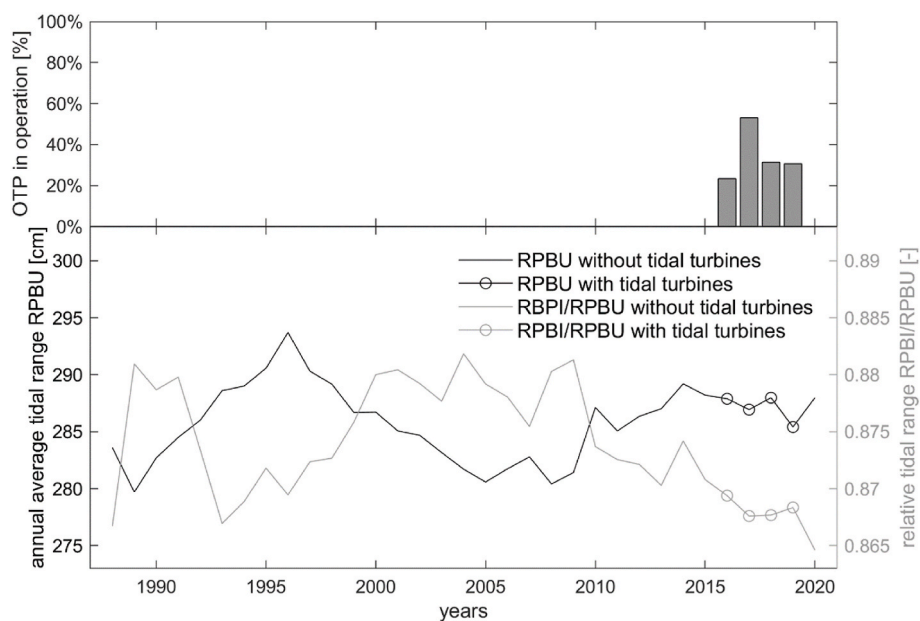

Fig. 4. Top: operational time per year of the tidal power plant (OTP). In the months September 2018 until April 2019, the OTP has been out of operation due to a break overhaul and in the year 2020 the OTP has not been out of operation due to bankruptcy of Tocardo Tidal Power B.V. The lower plot shows annual average tidal range for the station Roompot Buiten (RPBU) and the tidal amplification factor of Roompot Binnen (RPBI) for the situation with and without tidal turbines.

Table 1

Overview of ADCP measurements prior and after installation of the turbines. The position of the ADCPs are indicated in Fig. 3.

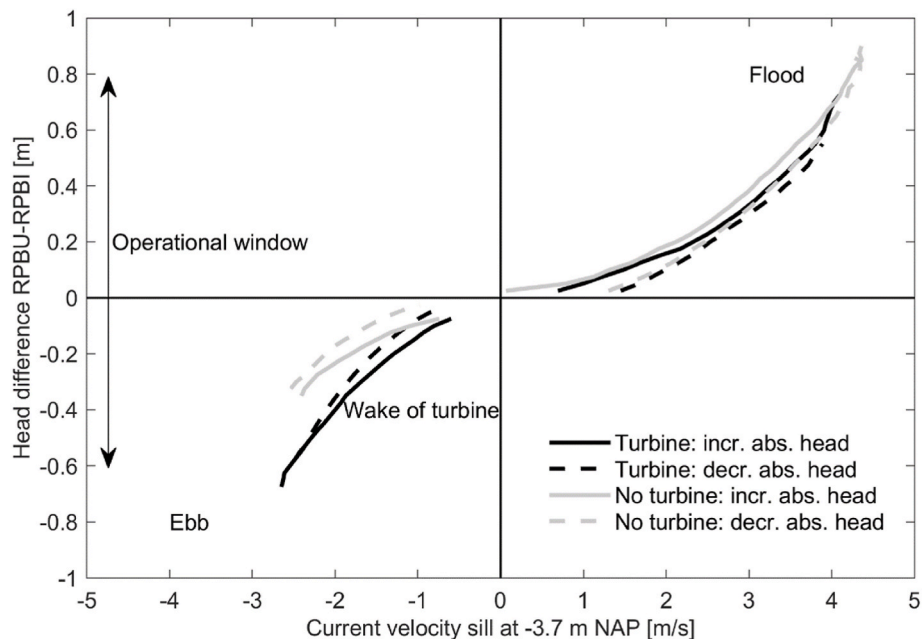| ADCP	Measuring period	days	Turbine operation	Range [m]	Beams	Beam angle	Orientation
2011V	15/08/2011–21/08/2011	6	–	9	2	20°	vertical
2011H	15/08/2011–21/08/2011	6	–	8.2	2	20°	horizontal
2016Hf	10/10/2016–26/10/2016	14	Normal	20	1	0°	horizontal
2016Hr	10/10/2016–26/10/2016	14	Normal	25	1	0°	horizontal

Fig. 5. Comparison of the 2011 vertical ADCP data without turbines with the ADCP data from the center turbine above the sill of the storm surge barrier at the height of the turbines for a period of 2 weeks. The lines show the median value. For ebb, the measurement plane (sill) is in the wake of the turbines.

by the shape of the sill of the barrier and the positioning of the tidal turbines at the Eastern Scheldt side of the barrier (Fig. 3). Without turbines, the measurement location of the vertical ADCP (ADCP2011V) is downstream of the sill during flood, such that the vertical ADCP measures the velocity of the contracted flow at this location due to flow separation at the front end of the sill beam (Fig. 6), while the measurement location is upstream of the sill during ebb, measuring uncontracted flow. For the situation with turbines, the measurement location at the sill is located downstream of the turbines during ebb, resulting in measuring in the wake of the turbine. During flood, the ADCP (ADCP2016Hf) measured the undisturbed flow velocity upstream of the turbine. This resulted in a larger inaccuracy in velocity measurements during ebb than during flood (see Fig. 5).

A more detailed analysis of the ADCP data is given by Verbeek et al. [29], who analyzed the difference in flow velocity with the turbines spinning in idle mode delivering a minimum of resistance to the flow. Verbeek et al. [29] also presented the measured velocities for the lateral beams of the ADCP. These measurements are not further discussed in this article as the measurement period of the multibeam measurements was only 1 day compared to the 16 days of measurement data for the one beam ADCP data as presented in Fig. 5.

No overlap in measurement location was available, due to the different orientation between the ADCP instruments in 2011, (which measured parallel to the barrier) and the ADCP instruments on the turbines, which measured perpendicular to the barrier (Fig. 3). The strong contraction of the flow towards the gates leads to a quickly developing flow profile close to the sill. This high variability of flow velocities combined with the absence of overlap in the measurements made it impossible to make a quantitative assessment of the resistance of the turbines on the flow through the barrier. However, to overcome this,

the measurement data was used to validate the CFD models which were run for the situations with and without turbines.

3.2. Numerical modelling

To assess the impact of the pilot plant on the environment (both nearfield and far-field), different types of modelling have been carried out. Nearfield modelling was carried out to directly assess the impact of the tidal turbines on the flow through the barrier and on the local bed protection and far-field modelling has been utilized to assess the impact of a reduced flow through the barrier on the intertidal area in the Eastern Scheldt basin.

3.2.1. Nearfield effects

To assess the impact of the tidal turbines on the environment, a CFD model (as described in Ref. [18]) was made extending 200 m at both sides of the barrier and consisting of 2 gates (Gate 8 and half the adjacent Gate 7 and Gate 9). The geometry of the storm surge barrier and the turbines including turbine blades were reproduced in detail. The bathymetry was based on a multibeam survey (0.5 m resolution) and converted to a resolution of 2 m in the model. Simulations were carried out for situations with and without turbines and the results were validated against the velocities measured by the ADCP measurement campaigns of both 2011 without turbines and 2016 with turbines installed (see Ref. [18]). In the simulations with turbines, the turbines were represented by means of an overset mesh, in which the actual rotation of the turbine blades was modelled. With these CFD models, four constant head conditions were modelled. For ebb, heads of 20 cm and 32 cm were simulated, while for flood heads of 20 cm and 55 cm were simulated. The two-phase simulations (air and water phases with Volume of Fluid

method) were carried out using the improved detached eddy simulation (IDDES) formulation, which uses Large-Eddy-Simulation (LES) in the bulk of the domain and the Reynolds-Averaged Navier–Stokes (RANS) approach near the bed and the walls. The imposed velocity profile at the inlet has been validated against velocity measurements at approximately 750 m upstream of the barrier in the Eastern Scheldt.

The validation of the CFD model has been described by O'Mahoney et al. [18], covering validation against velocity, thrust and power measurements. Although this model was not able to cover the inertia effect as observed in the measurements, the model was able to assess the effect of the turbines on the discharge coefficient. The discharge co-efficients (μ) were calculated by means of the water level difference (Δh in m) over the model and the computed discharges (Q in m^3/s) at the sill by the CFD model by the following formula:

$$Q = \mu A \sqrt{2g\Delta h} \tag{1}$$

Where g (m/s^2) is the gravitational acceleration and A (m^2) the throughflow area between the sill and the water level. A reduction of about 0.05 in the discharge coefficient was found during ebb, while no reduction in the discharge coefficient was found during flood (Table 2). This is mainly caused by the position of the turbines with respect to the sill of the barrier. The turbines are located at the Eastern Scheldt side of the barrier. During flood, the flow is influenced by the turbines after passing and detached from the sill. This is different for ebb, where the flow is influenced by the turbines before the sill of the barrier is reached (Fig. 3). In the flood cases the wakes of the turbines are situated in the outflow of the barrier and do not affect the discharge coefficient, while in the ebb cases the wakes of the turbines are part of the inflow to the barrier and result in a reduction of the discharge coefficient of the gate in question.

The CFD model simulations were also used to assess the impact of the turbulence generated by the turbines on the bed protection. In Fig. 6, a vertical cross-section of the CFD generated flow field is shown for the situation with and without turbines for a head difference of 20 cm during flood. This figure shows difference in time-averaged flow ve-locities directly downstream of the turbines. For the situation without turbines, flow contraction takes place at the sill after which the flow remains attached to the water surface. After approximately 100 m, the

Table 2
Discharge coefficients through the gate with turbines (Gate 8) and through the lateral gates without turbines.

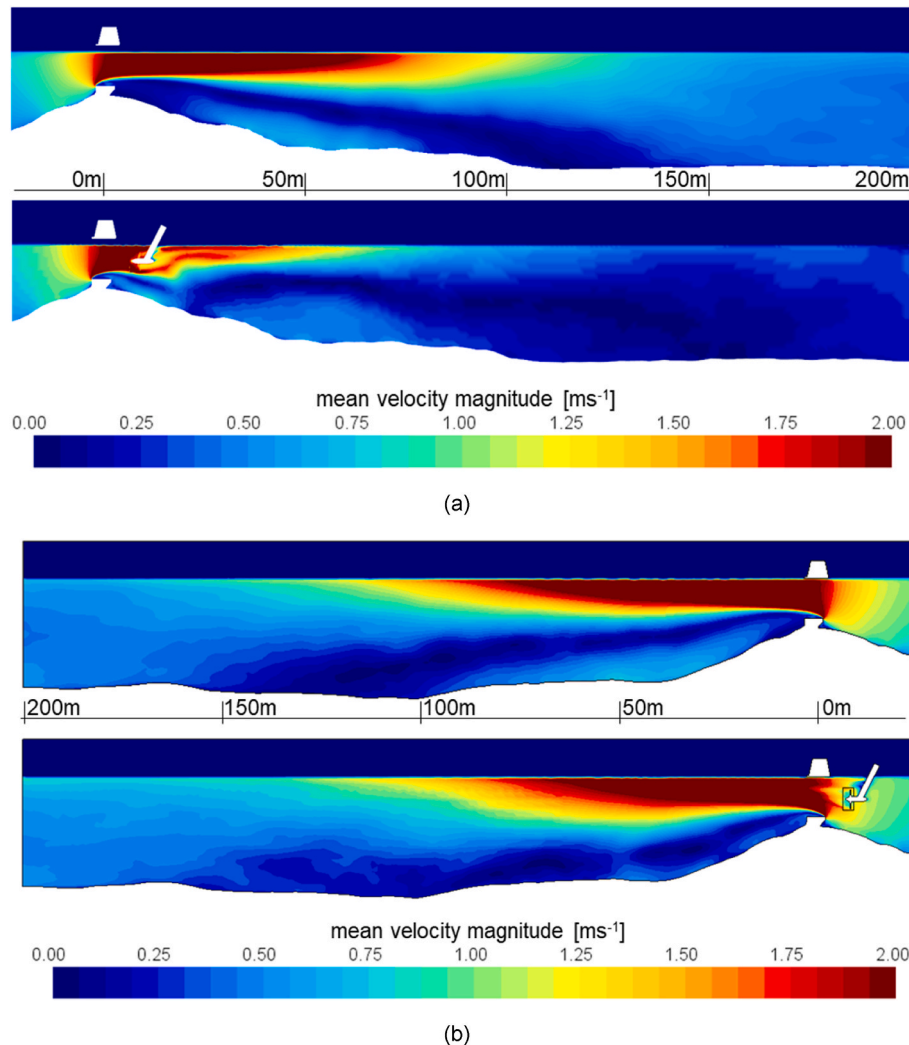|	Case	Head [m]	Discharge coefficient		
			Lateral gates	Gate 8	difference
Ebb	1	−0.2	0.97	0.93	0.05
	2	−0.32	0.98	0.92	0.06
Flood	3	0.2	0.85	0.85	0
	4	0.55	0.88	0.88	0

(a)

(b)

Fig. 6. Mean velocity at a vertical cross section through turbine 2 for (a) flood simulation and (b) ebb simulation with a head difference of 0.2m. The top panels show the velocity magnitude for the situation without turbines and the lower panels show the velocity magnitude with turbines.
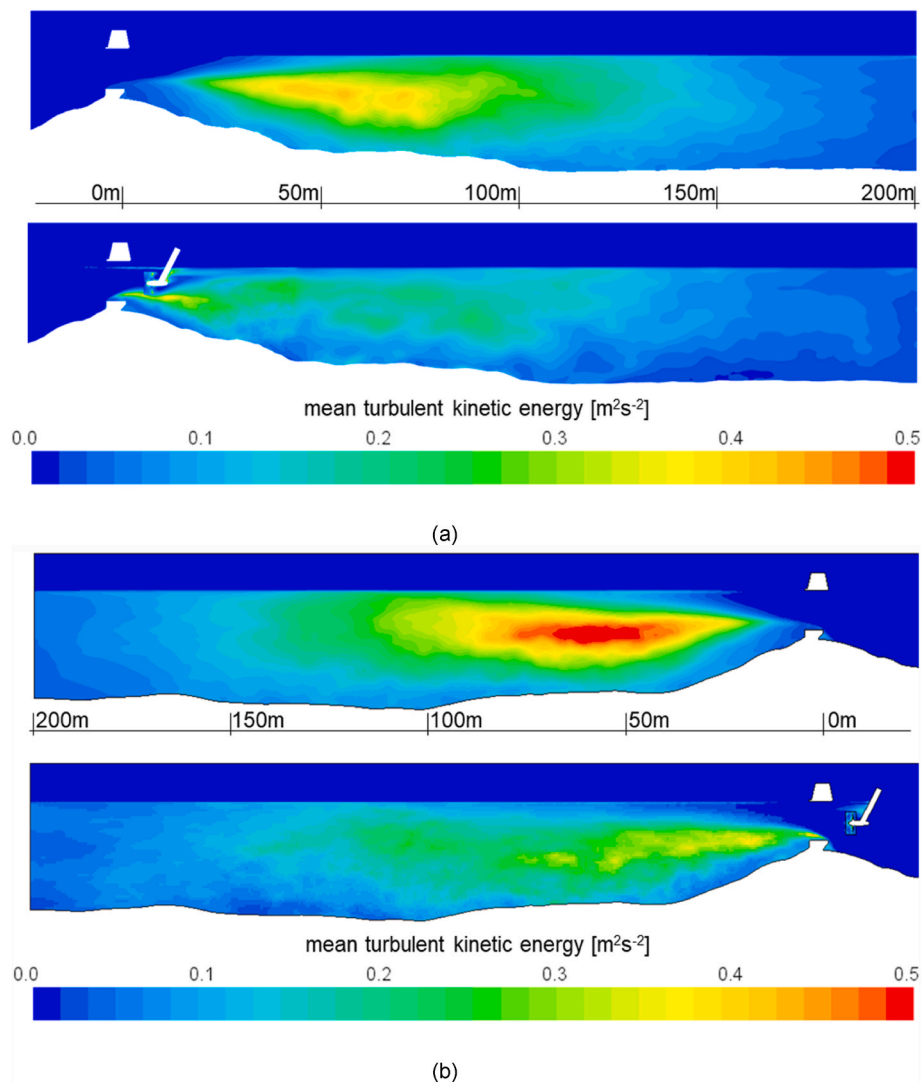
Fig. 7. Mean turbulent kinetic energy (TKE) at a vertical cross section through turbine 2 for (a) flood simulation and (b) ebb simulation with a head difference of 0.2m. The top panels show the TKE for the situation without turbines and the lower panels show the TKE for the situation with turbines.

flow starts to spread over the whole water column. This is different for the situation with turbines, where the turbines "absorb" a large part of the kinetic energy of the flow near the surface. The flow velocity in the upper water column behind the turbines is significantly lower, resulting in a weaker shear zone between the upper and lower water layers. The smaller flow velocity for the case with turbines resulted in a large zone with lower flow velocities near the bed, except for the return flow in the first 20 m in the flood simulation (Fig. 6).

The difference in turbulent fluctuations at the same cross section is shown in Fig. 7 in terms of the turbulent kinetic energy. Significant differences are found behind the turbines and small differences can be observed near the bed for the situation with and without turbines. The high turbulence intensity for the situation without turbines is generated by the obstruction of the sill and the pillars of the barrier.

As seen in Figs. 6 and 7, the turbines influence the flow patterns behind the barrier significantly. The turbines reduce the strength of the shear layer which is formed by the flow detachment from the sill. This results in a lower turbulence intensity behind the turbines than compared to without turbines. A similar effect is observed at the North Sea side of the barrier in case of ebb. However, this effect is smaller, as the sill is located downstream of the turbines for this situation. The change in average flow velocities and turbulence intensity behind the turbines influences the loads on the bed protection. Based on the CFD

model results at 100 m from the barrier, the average velocities at the bed remained similar or decreased (by max 0.1 m/s) due to the presence of the turbines and the velocity fluctuations decreased as well in all simulated situations (by max 0.15 m/s). Based on general stability formulas for bed protection (see e.g. Ref. [30]), lower flow velocities and velocity fluctuations lead to reduced loads on the bed protection. It is important to note that these results are averaged results. At some locations, the velocities and velocity fluctuations slightly increased. However, in general a decreasing trend was observed in mean velocity and velocity fluctuations near the bed with the turbines installed.

3.2.2. Far-field effects

The impact of the additional resistance by the turbines on the flow through the barrier has been studied by large scale depth-averaged hydrodynamic models. The model, which is shown in Fig. 1 covers a large part of the ebb-tidal delta and the complete Eastern Scheldt tidal basin [19,20] The model has been built with Delft3D-FLOW [31] and has been validated with data from the water level measuring stations in the Eastern Scheldt (Fig. 1). Each gate was represented by one cell with a width of 45 m (the actual gate opening is 39.5 m, with a pillar width of 5.5 m) and the local depth at the sill. The flow rate through the barrier (and tidal turbines) were represented by means of a discharge relation represented by an additional quadratic friction term in the momentum

Table 3

Root mean square (RMS) errors of the water levels of the hydrodynamic model at the measuring stations. The stations OS11 and Roompot Buiten are located at the North Sea side, the other stations are in the Eastern Scheldt basin.

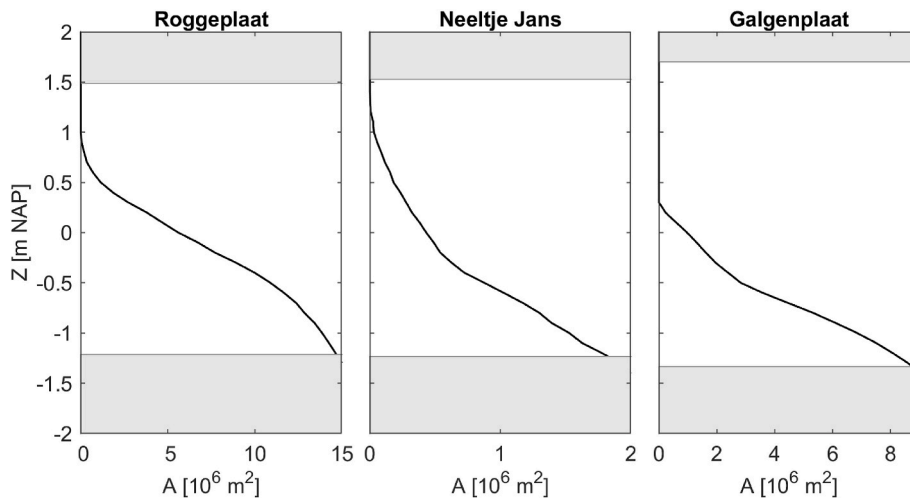| Station	distance from barrier [km]	tidal range [m]	RMS error [m]
			year 2014
OS11	−14	3.01	0.081
Roompot buiten (RPBU)	<-0.5	2.98	0.087
Roompot binnen (RPBI)	<0.5	2.61	0.109
Stavenisse (STAV)	22	2.73	0.102
Yerseke (YE)	32	2.98	0.108
Marollegat (MRG)	43	3.48	0.112

Fig. 8. Hypsometric curves of the Roggeplaat, Neeltje Jans and the Galgenplaat (for locations, see Fig. 1) derived from the model bathymetry. The white areas represent the intertidal window at the tidal flat.

equation, also known as "porous plates". The porous plates were placed on both sides of the barrier, meaning that each gate contains two porous plates and a sill. The porous plates in the gate with turbines were tuned to match the computed discharge loss of the CFD simulations. Delft3D is not able to account for different discharge coefficients for ebb and flood. For this reason, one value was selected for the loss in discharge co-efficients, which is similar for ebb and flood.

The hydrodynamic model was validated using measured water levels inside and outside the basin. The stations Roompot Binnen, Stavenisse, Yerseke and Marollegat were selected for the validation in the Eastern Scheldt basin and the stations Roompot Buiten and OS11 were selected for the validation at the North Sea side (Fig. 1). The validation was carried out for the year 2014. The model was able to represent the measured water levels with an accuracy of 10–11 cm inside the basin and 8–9 cm on the North Sea side of the barrier (Table 3).

The impact on the flow around the Roompot section of the barrier, has been assessed for the operational head of the tidal power plant, which is 0.8 m during flood and 0.6 m during ebb. For this situation, the maximum differences between the simulations with turbines and without turbines are compared for depth averaged flow velocities and flow direction. Differences in depth-averaged velocity up to 3 cm/s were found at velocity magnitudes of approximately 1.0 m/s. These differ-ences reached up to about 1 km from the barrier, exceeding the edge of the bed protection at 600 m from the barrier. The difference in velocity direction for the situation with and without turbines was approximately 10°. This change in velocity direction occurred mainly near the turning of the tide during low heads and low flow velocities. For the higher hydraulic heads, no change in flow direction was observed between the situations with or without turbines.

To assess the impact of the tidal turbines on the intertidal areas in the Eastern Scheldt, the water level deviation at the most important inter-tidal flats was assessed: the Roggeplaat, Neeltje Jans and the

Galgenplaat (Fig. 1). A reduction in flow through the barrier leads to a decrease in tidal range, resulting in a smaller intertidal area. The intertidal area for these three tidal flats is shown by means of the hyp-sometric curves in Fig. 8.

While the impact on the water levels in the Eastern Scheldt is small with turbines installed in Roompot Gate 8 only, model simulations were also carried out for the situation with turbines installed in each of the 62 gates of the barrier. Although this is an unrealistic scenario, it does provide information about a maximum potential impact. Based on the results of the CFD model simulations, the tidal turbines in Roompot 8 induced a decrease in discharge coefficient of 5% for ebb. No changes were found during flood. However, different positioning of the turbines, different operation of the turbines, or different turbine designs may lead
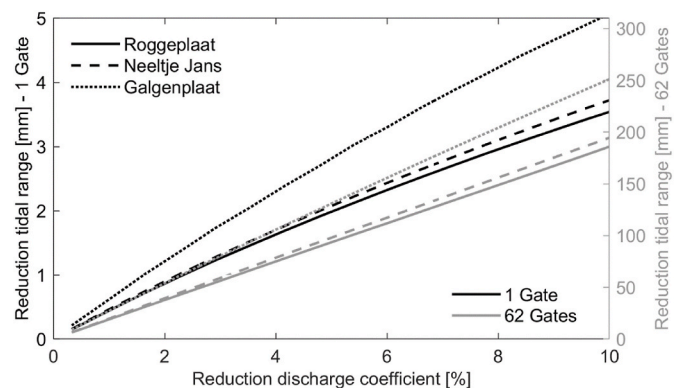

Fig. 9. Reduction in tidal range at the intertidal flats with turbines installed in 1 gate (black lines) and with turbines installed in all 62 gates (grey lines). The right-hand axis is an exact scaling of the left hand axis with a factor 62.

to a different impact on the discharge coefficient. For this reason, various model simulations were carried out for reductions in discharge coefficient up to 10%. The applied reduced discharge coefficients were similar for both ebb and flood. It has to be noted that the levels of the sill vary between the gates, which would result in smaller tidal turbines in the gates near the headlands with a different power output. No variation of the power over the width of the storm surge barrier was used in these simulations. Furthermore, the simulations did not include an operational head limitation, i.e. the turbines could operate up to the maximum occurring head. Based on the simulations that were carried out with the hydrodynamic model with tidal turbines installed in Gate 8 only, the tidal range at the most important tidal flats (Roggeplaat, Neeltje Jans and the Galgenplaat) reduced with approximately 2–3 mm for a reduction of 5% in discharge coefficient (Fig. 9), which results in an instantaneous reduced intertidal area of between 0.2 ha and 0.5 ha (Fig. 10), which is less than 0.1% of the tidal flat area. The total intertidal area of the Eastern Scheldt Estuary was approximately 11.000 ha in 1986 (reference year for start of monitoring autonomous negative trends). A similar analysis was carried out for the situation whereby turbines are installed in all 62 gates. In Figs. 9 and 10, the reduction in

intertidal area and the reduction in tidal flat area is shown for the different tidal flats. Considering a reduction of 5% in discharge coefficient, the reduction in tidal range would reach up to 13 cm at the Galgenplaat. This leads to a reduction of intertidal area of 25 ha, which is about 3% of this tidal flat.

In Fig. 11, the reduction in tidal flat area is shown against the number of gates in which tidal turbines are installed. In this analysis, a reduction in discharge coefficient of 5% is applied for respectively 1, 4, 8, 16, 31 and 62 gates. The gates involved are evenly distributed over the barrier, with Roompot Gate 8 as single gate. The variation in tidal range also induces a small variation in mean sea level. This variation is less than 1 mm at these tidal flats for all simulations and can be ignored.

The sediment starvation and the blockage of the gates by tidal turbines are not the only stressors that causes a reduction in intertidal area in the Eastern Scheldt basin. Sea level rise results in an increase of the mean low water level (MLW), which results in a reduction of the intertidal area as well (see Fig. 2). For the Eastern Scheldt basin, different sea level rise scenarios were defined by the KNMI (Royal Dutch Meteorological institute – see van den Hurk et al. [32]). These scenarios were based on a global temperature increase of 1–2 °C temperature increase for the period 1990–2050. Because the installation of the tidal turbines leads to an instantaneous increase in low water level, the impact can be considered constant, while sea level rise is a continuing process. Considering an average scenario for sea level rise as defined by van den Hurk et al. [32], the sea level would rise by 25 cm for the period 1990–2050, or 4.17 mm/year on average. For the simulations, the assumption is made that MLW increases by the same amount as mean sea level as defined by van den Hurk et al. [32]. Comparing this increase in mean low water level with the impact of the tidal turbines in Roompot Gate 8 (Fig. 12), a sea level rise of 3.5 months has a similar effect on the mean low water level in the Eastern Scheldt basin compared to the pilot plant in Roompot Gate 8. It should be noted that this loss is reversible and can be made undone by decommission the pilot plant.

In Fig. 12, the impact on the mean low water level at the Galgenplaat is shown for various number of gates filled with turbines. In this analysis, a worst-case scenario is shown in which all gates are filled with turbines. Besides the impact on intertidal area, such a scenario may have a significant effect on the ecology, as it could complicate fish and sea mammal migration through the barrier [33]. In such a situation, the barrier with tidal stream turbines would face similar challenges compared to tidal lagoons and tidal barrages (see e.g. Ref. [34]).
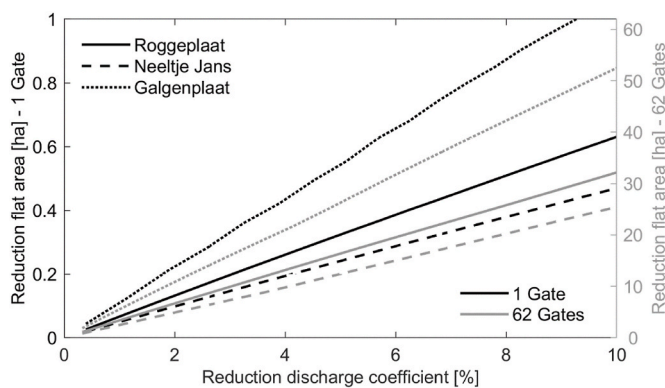

Fig. 10. Reduction in intertidal area at the intertidal flats with turbines installed in 1 gate (black lines) and with turbines installed in all 62 gates (grey lines). The right-hand axis is an exact scaling of the left hand axis with a factor 62.
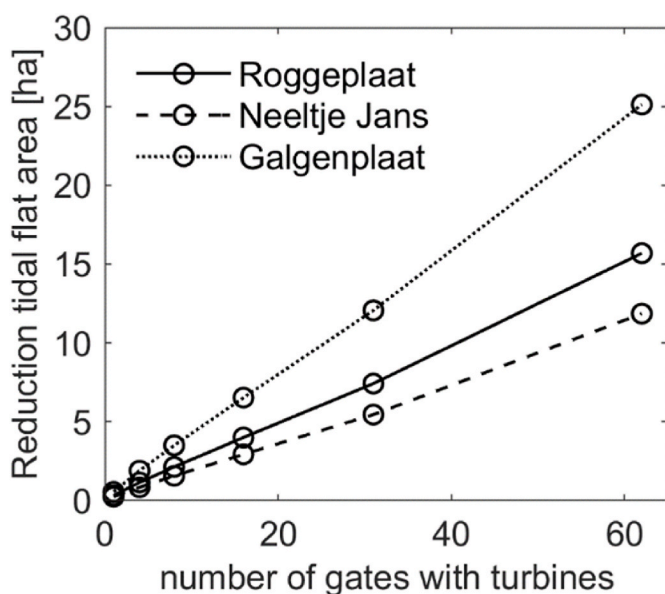

Fig. 11. Reduction in intertidal area at the intertidal flats for different gates with tidal turbines installed. This analysis considers a reduction in discharge coefficient of 5%.
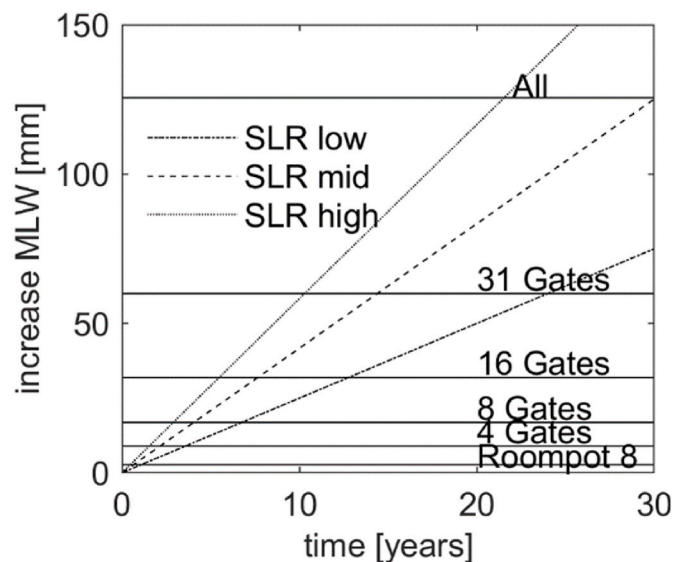

Fig. 12. Impact of three sea level rise (SLR) scenario's compared to the impact of tidal turbines (5% resistance) on the mean low water level at the Galgenplaat.

To prevent the intertidal flats in the Eastern Scheldt from drowning, a large suppletion of 1.3 million m³ of sand took place, where sand from the Roompot tidal channel was dumped on the Roggeplaat at the end of 2019. This suppletion with an average height of 9 cm should preserve the tidal flat for 25 years [27]. Comparing this to the higher mean low water level by the turbines in Roompot gate 8, the turbines would reduce the effective time of the suppletion by approximately 4 months. Installation of turbines in all gates (see Fig. 9) would reduce the effective time by approximately 15 years.

4. Discussion

Although extensive monitoring campaigns were setup where water levels and flow velocities were measured in detail near the pilot plant in Eastern Scheldt barrier, it was not possible to directly quantify the impact of the pilot plant based on these measurements alone. To quantify the impact of the pilot plant, numerical nearfield and far-field models were used and validated against the water level and ADCP velocity measurements. By means of the nearfield CFD model, the impact of the pilot plant on the flow through the barrier and the impact on the bed protection was determined. By using the additional resistance of the turbines on the flow through the barrier in the large-scale model, the impact on the intertidal areal was assessed, which is one of the key aspects of a healthy ecosystem in the Eastern Scheldt (Fig. 2).

The impact of the pilot plant on the tidal range in the Eastern Scheldt was difficult to determine compared to the natural variation in head over 18.6 years. As the pilot plant was only in operation for a maximum of 50% of the time, due to the limit in operational head and maintenance works, the impact of the pilot plant should be judged separately from the natural variation. Longer measurement periods are required to assess the impact on the tidal range quantitatively. The numerical far-field model predicts a decrease of a few millimeters in tidal range at the main tidal flats. However, in these simulations, the limited operational window was not incorporated, and a similar resistance was present for both ebb and flood, while this is different for the pilot plant. These assumptions result in an overprediction of the impact on the tidal range in the estuary by the numerical model.

By means of the nearfield CFD model, a detailed insight is obtained in the flow behavior near the bed protection. These detailed insights in flow patterns near the bed can provide valuable information for the impact on the bed protection. At present most bed protections near hydraulic structures are designed based on depth average flow velocity fields combined with a turbulent kinetic energy amplification factor.

Although the storm surge barrier seems a good place for extracting tidal energy, a possible upscaling of tidal power from the Eastern Scheldt storm surge barrier requires dedicated investigations as to the positioning of the turbines with respect to the sill as this will determine the impact of the turbines on the flow through the barrier. Besides the positioning of the turbines, the sill level varies over the width of the barrier, which makes not every opening equally suitable for harvesting tidal energy. Additionally, increasing the blockage of specific gates by tidal turbines might influence the flow through the adjacent gates. The blockage owing to the turbines leads to a slightly increased water level upstream of the gate with turbines and adjacent gates and a slower filling of the inner basin, which results in a higher discharge trough the remaining gates. Such an effect was indeed noticed in the results of the CFD simulations during ebb and it will be present in the far-field model, especially when multiple gates are filled with turbines. As the Eastern Scheldt consists of 3 sections with gates (Fig. 1), the installation of tidal turbines in the Roompot section might lead to increased flow velocities at the Schaar section and at the Hammen section. An unequal distribution of tidal energy extraction from this barrier might also result in changes in flow patterns at locations where turbines are absent. Variations in positioning of turbines with respect to the sill, or the size of the turbines and the unequal distributions of turbines over the width of the barrier are not considered in this article. However, optimization routines could be used to find an optimal configuration considering power output and environmental constraints (see Ref. [15]).

An environmental problem in the estuary is the erosion of the ecologically valuable intertidal flats. The erosion since the building of the storm surge barrier is caused by the weakening of the tidal flow in the channels [23]. Tidal power extraction at the barrier can further reduce the strength of the tidal flow in the channels aggravating this environmental problem. However, after the building of the storm surge barrier the tidal flow is hardly able to transport any sediment to the tidal flats. Therefore, the impact of the considered tidal power extraction on this aspect is expected to be very limited.

5. Conclusion

Hydraulic structures like storm surge barriers are ideal locations to harvest tidal energy. Besides the high flow velocities that occur near these structures, easy access for installation and maintenance and a close connection to the grid are obvious advantages. However, as most existing hydraulic structures are not designed for harvesting tidal energy, thorough investigations are required to understand the potential impacts on flood protection and environment before larger schemes can be considered.

This paper discusses the impact of the tidal turbines in the Eastern Scheldt Storm Surge Barrier on barrier safety by assessing the impact of the flow on the bed protection near the barrier and on the environment by assessing the development of the intertidal flats in the Eastern Scheldt, which are a key factor in the ecosystem.

The local effects of the array of five tidal turbines in Gate 8 of the Roompot section of the Storm Surge Barrier are small. By means of a monitoring campaign, numerical models were validated which were used to assess the impact of the pilot plant on the bed protection near the barrier and on the intertidal areal of the Eastern Scheldt estuary. It was not possible to detect the impact of the pilot plant on the tidal range in the estuary compared to the natural variation in tidal range over 18.6 years. A CFD model was built and validated against the measured velocities near the pilot plant. By means of this CFD model, it was shown that the turbines of the pilot plant in Gate 8 had no impact on the flow through the barrier during flood, while a decrease in discharge of 5% was found during ebb. The simulations showed that the turbulent velocity fluctuations were smaller at most locations near the bed protection when tidal turbines were installed, as the tidal turbines reduce the strength of the turbulent eddies coming from the sill of the barrier. However, at other locations the velocities and velocity fluctuations slightly increase. The overall impact on the bed protection was therefore considered to be neutral for this pilot plant. In case of upscaling when multiple gates are filled with tidal turbines, the flow velocities in the gates without turbines might change which could change the loads at the bed protection of these gates. The CFD simulations covered stationary situation within the operational limits of the plant. The influence of the turbines for hydraulic heads outside the operational head limitations were not considered.

The impact on the main intertidal flats in the Eastern Scheldt by the tidal turbines in the barrier was assessed by a large-scale hydrodynamic model for different scenarios in which multiple gates were equipped with tidal turbines. The impact on the tidal range and the intertidal areas of the ecological sensitive Eastern Scheldt estuary ranged from very small for the pilot plant in Gate 8 to substantial in case turbines are placed in all gates. Comparing this to an average sea level rise scenario, the installation of tidal turbines in Gate 8 of the Eastern Scheldt is equivalent to the sea level rise of 3.5 months. Rijkswaterstaat preserves the tidal flats by suppletion's to compensate for effects of sea level rise. Based on a profit principle, it could be argued that tidal energy extraction from the storm surge barrier should compensate for the loss in intertidal area. However, it should be noted that the loss in intertidal area would be immediately restored at the end of the project life upon removal of the turbines.

The detailed measurements that were taken at the pilot plant in the Eastern Scheldt showed that validation of the applied numerical models gives the required insights to understand the hydraulic impact of the TEC array on the hydraulic structure. This understanding is needed for extra credibility of the predictions of the extrapolated large-scale and large array assessments which are always going to be fully numerical.

CRediT authorship contribution statement

Anton de Fockert: Conceptualization, Investigation, Visualization, Writing – original draft. **Arnout C. Bijlsma:** Supervision, Writing – review & editing. **Tom S.D. O'Mahoney:** Investigation, Validation. **Wilbert Verbruggen:** Investigation. **Peter C. Scheijgrond:** Funding acquisition, Supervision. **Zheng B. Wang:** Supervision.

Declaration of competing interest

The authors declare that they have no known competing financial interests or personal relationships that could have appeared to influence the work reported in this paper.

Acknowledgements

References

[1] W. Krewitt, C. Klessman, C. Capone, E. Stricker, W. Graus, M. Hoogwijk, N. Supersberger, U. Von Winterfeld, S. Samadi, Role and potential of renewable energy and energy efficiency for global energy supply, Climate Change 18/2009, Report-no. (UBA-FB) 001323/E, ISSN 1862-4359, Part II, 71-131, Published by Federal Environment Agency, Dessau-Rosslau.

[2] R. Pelc, R.M. Fujita, Renewable energy from the ocean, J. Mar. Policy 26 (2002) 471–479, https://doi.org/10.1016/S0308-597X(02)00045-3.

[3] A.S. Bahaj, Generating electricity from the oceans, J. Renew. And Sustain. Energy. Revis 15 (2011) 7, https://doi.org/10.1016/j.rser.2011.04.032, 3399-3416.

[4] A.G.L. Borthwick, Marine renewable energy seascapes, J. Eng. 2 (2016) 69–78, https://doi.org/10.1016/J.ENG.2016.01.011.

[5] S.P. Neill, J.R. Jordan, S.J. Couch, 2012. Impact of tidal energy converter (TEC) arrays on the dynamics of headland sand banks, Renew. Energy 37 (2012) 387–397, https://doi.org/10.1016/j.renene.2011.07.003.

[6] M.A. Shields, D.K. Woolf, E.P.M. Grist, S.A. Kerr, A.C. Jackson, R.E. Harris, M. C. Bell, R. Beharie, A. Want, E. Osalusi, S.W. Gibb, J. Side, Marine renewable energy: the ecological implications of altering the hydrodynamics of the marine environment,, J. Ocean & Coast. Manag 54 (1) (2010) 2–9.

[7] A. Chatzirodou, H. Karunarathna, D.E. Reeve, 3D modelling of the impacts of in-stream horizontal-axis Tidal Energy Converters (TECs) on offshore sandbank dynamics, J. Appl. Ocean. Res 91 (2019), 101882, https://doi.org/10.1016/j.apor.2019.101882.

[8] I. Fairley, I. Masters, H. Karunarathna, The cumulative impact of tidal stream turbine arrays on sediment transport in the Pentland Firth,, Renew. Energy 80 (2015) 755–769, https://doi.org/10.1016/j.renene.2015.03.004.

[9] P.E. Robins, S.P. Neill, M.J. Lewis, Impact of tidal-stream arrays in relation to the natural variability of sedimentary processes, Renew. Energy 72 (2014) 311–321, https://doi.org/10.1016/j.renene.2014.07.037.

[10] R. Ahmadian, R.A. Falconer, Assessment of array shape of tidal stream turbines on hydro-environmental impacts and power output, Renew. Energy 44 (2012) 318–327. http://doi:10.1016/j.renene.2012.01.106.

[11] D. Fallon, M. Hartnett, A. Olbert, S. Nash, The effect of array configuration on the hydro-environmental impacts of tidal turbines,, Renew. Energy 64 (2014) 10–25, https://doi.org/10.1016/j.renene.2013.10.035.

[12] D.R. Plew, C.L. Stevens, Numerical modelling of the effect of turbines on currents in a tidal channel – Tory Channel, New Zealand, Renew. Energy 57 (2013) 269–282, https://doi.org/10.1016/j.renene.2013.02.001.

[13] V. Ramos, R. Carballo, M. Alvarez, M. Sanchez, G. Iglesias, Assessment of the impacts of tidal stream energy through high-resolution numerical modelling, J. Energy 61 (2013) 541–554, https://doi.org/10.1016/j.energy.2013.08.051.

[14] M. Sanchez, R. Carballo, V. Ramos, G. Iglesias, Tidal stream energy impact on the transient and residual flow in an estuary: a 3D analysis,, J. Appl. Energy 116 (2014) 167–177, https://doi.org/10.1016/j.apenergy.2013.11.052.

[15] E. González-Gorbeña, A. Pacheco, T.A. Plomaritis, Ó. Ferreira, C. Sequeira, Estimating the optimum size of a tidal array at a multi-inlet system considering environmental and performance constraints, J. Appl. Energy 232 (2018) 292–311, https://doi.org/10.1016/j.apenergy.2018.09.204.

[16] Irena, Innovation Outlook – Ocean Energy Technologies, Int. Renew, Energy Agency, Abu Dhabi, 2020. ISBN 978-92-9260-287-1, https://www.irena.org/publications/2020/Dec/Innovation-Outlook-Ocean-Energy-Technologies.

[17] M. Leopold, M. Scholl, Monitoring Tidal Turbines Eastern Scheldt Storm Surge Barrier, annual report, Wageningen University and Research report C010/19, 2018, https://doi.org/10.18174/470409. in Dutch.

[18] T.S.D. O'Mahoney, A. de Fockert, A.C. Bijlsma, P. de Haas, Hydrodynamic impact and power production of tidal turbines in a storm surge barrier, Int. Mar. Energy. J 3 (3) (2020), https://doi.org/10.36688/imej.3.127-136.

[19] K. Guijt, Impact of Tidal Energy Extraction in the Eastern Scheldt Storm Surge Barrier on Basin Hydrodyanamics and Morphology, Delft University of Technology M.Sc, thesis, 2018. http://resolver.tudelft.nl/uuid:d81e9586-a3a9-4000-a4d8-6a6ea22f4022.

[20] M. Eelkema, Eastern Scheldt Inlet Morphodynamics, PhD thesis Delft University of Technology, 2013. ISBN 978-90-9027347-1.

[21] M. Jeuken, On the Morphologic Behaviour of Tidal Channels in the Westerschelde Estuary, Ph.D. thesis, Universiteit Utrecht, 2000. ISBN 90-6266-192-0.

[22] J. van Veen, A.J.F. van der Spek, M.J.F. Stive, T. Zitman, Ebb, Flood Channel, Systems in The Netherlands tidal waters, J. Coast. Res. 21 (6) (2005) 1107–1120, https://doi.org/10.2112/04-0394.1.

[23] P.L.M. de Vet, B.C. van Prooijen, Z.B. Wang, The differences in morphological development between the intertidal flats of the Eastern and Western Scheldt, J. Geom. 281 (2016) 31–42, https://doi.org/10.1016/j.geomorph.2016.12.031.

[24] Design Rijkswaterstaat, Plan Oosterschelde Storm-Surge Barrier – Overall Design and Design Philosophy, A.A. Balkema, Rotterdam, 1994. ISBN 90 5410 1075.

[25] T. Louters, J.H. van den Berg, J.P.M. Mulder, Geomorphological changes of the Oosterschelde tidal system during and after the implementation of the delta project, J. Coast. Res. 14 (3) (1998) 1134–1151.

[26] J.P.M. Mulder, T. Louters, Changes in basin geomorphology after implementation of the Oosterschelde estuary project, J. Hydrobiol. 282/283 (1994) 29–39.

[27] J.J. van der Werf, P.L.M. de Vet, M.P. Boersema, T.J. Bouma, A.J. Nolte, R. A. Schrijvershof, L.M. Soissons, J. Stronkhorst, E. van Zanten, T. Ysebaert, An integral approach to design the Roggenplaat intertidal shoal nourishment, J Ocean and Coast, Man 172 (2019) 30–40, https://doi.org/10.1016/j.ocecoaman.2019.01.023.

[28] J.G. de Ronde, J.P.M. Mulder, L.A. van Duren, T. Ysebaert, Final advise autonomic downward trend eastern Scheldt (in Dutch). http://publicaties.minienm.nl/documenten/eindadvies-ant-oosterschelde, 2013, 1207722-000-ZKS-0010.

[29] M.C. Verbeek, R.J. Labeur, W.S.J. Uijttewaal, The performance of a weir-mounted tidal turbine: field observations and theoretical modelling,, Renew. Energy 153 (2020) 601–614, https://doi.org/10.1016/j.renene.2020.02.005.

[30] B. Hofland, Rock and Roll – Turbulence-Induced Damage to Granualrr Bed Protections, PhD thesis Delft University of Technology, 2005. ISBN 9789090201221.

[31] Deltares, Delft3D-FLOW user manual - simulation of multi-dimensional hydrodynamic flows and transport phenomena, including sediments, Version: 3.15, SVN Revision 68861 (2020). https://content.oss.deltares.nl/delft3d/manuals/Delft3D-FLOW_User_Manual.pdf.

[32] B. van den Hurk, A.K. Tank, G. Lenderink, A. van Ulden, G.J. van Oldenborgh, C. Katsman, H. van den Brink, F. Keller, J. Bessembinder, G. Burgers, G. Komen, W. Hazeleger, S. Drijfhout, New climate change scenarios for The Netherlands, J Water Sci. Technol. 56 (4) (2007) 27–33, https://doi.org/10.2166/wst.2007.533.

[33] R. Kastelein, N. Jennings, Effects of the Eastern Scheldt Storm Surge Barrier and tidal energy turbines on harbor porpoise (Phocoena phocoena) and harbor seal (Phoca vitulina) movements, SEAMARCO report (2019-01). https://tethys.pnnl.gov/sites/default/files/publications/Kastelein-2019-Tidal.pdf.

[34] Review Decc, Of tidal lagoons, department of energy and climate change. https://www.gov.uk/government/publications/1-severn-tidal-power-feasibility-study-conclusions-and-summary-report, 2010.